Covalently introducing sulfur in a thiol-rich metal-organic framework toward advanced lithium-sulfur batteries

Shangjun Lin,[a] Hujing Zhou,[a] Ruwei Chen,[a] Xuanhe Hu*,[a] and Jun He*,[a]

[a] *School of Chemical Engineering and Light Industry, Guangdong University of Technology, Guangzhou, Guangdong 510006, China*
Email: huxh@gdut.edu.cn (X. Hu); junhe@gdut.edu.cn (J. He)

Abstract The severe shuttle effect and sluggish reaction kinetics have hindered the commercial application of high-energy lithium-sulfur (Li-S) batteries. In this work, a dual-thiol metal-organic framework (MOF) was in situ synthesized on carbon nanotubes, and sulfur was covalently connected to this composite (UiO-66(SH)$_2$@CNT) to form a MOF-sulfur copolymer (S-UiO-66(SH)$_2$@CNT). Benefiting from the strong covalent interaction between thiol groups and sulfur species, the S-UiO-66(SH)$_2$@CNT cathode can retard the shuttle effect and simultaneously strengthen the redox kinetics of polysulfides. As a result, a discharge capacity of 791 mAh g^{-1} is achieved at a current density of 0.2 C, whereas the S/UiO-66@CNT cathode using the blend of UiO-66@CNT and sulfur as active materials only shows a specific capacity of 670 mAh g^{-1}. Moreover, the S-UiO-66(SH)$_2$@CNT cathode exhibits a higher capacity retention of 93.27 % at 0.5 C during 200 cycles compared with that of the S/UiO-66@CNT cathode (64.94 %). This work will provide significant inspiration for the design of advanced MOFs and cathodes for excellent Li-S batteries.

Keywords Metal-organic framework, Lithium-sulfur battery, Thiols, Shuttle effect, Reaction kinetics

Introduction

High energy battery is more and more demanded with the rapid development of portable electronic devices and new energy vehicles over the past few decades. Lithium-sulfur batteries as one of the most promising next-generation battery technologies, have received increasing attention owing to their high gravimetric energy density and discharge capacity.[1-5] However, the practical application of Li-S batteries is impeded by various issues including the poor conductivity of sulfur and lithium sulfide, massive volume expansion of sulfur upon lithiation, severe shuttle effect of polysulfide intermediates, and the sluggish reaction kinetics.[6-11]Specifically, the shuttle effect resulted from polysulfide dissolution/diffusion, and the sluggish conversion process between different polysulfide species during charging and discharging results in low sulfur utilization and poor cycling stability.[12-16]

Tremendous efforts have been made to solve these problems and a common strategy is to use porous materials as hosts to confine sulfur in the cathode. So far, a variety of porous carbon-based hosts have been developed to physically encapsulate sulfur and improve the conductivity of active species.[17-20] However, the weak van der Waals interaction between carbon and polysulfides limits their application. To enhance the interaction between sulfur and host, covalently introducing sulfur in the host to form a copolymer has been developed. When heated at an appropriate temperature (159-245 °C), the circle sulfur (S_8) molecules could transform to linear sulfur chains via a ring-opening reaction. After copolymerizing with hosts, the sulfur-host copolymer can be obtained. For instance, Yan et al. reported a sulfur cathode by the covalent attachment of sulfur to the thiol-functionalized graphene.[21] Similarly, Gao et al. used the thiol-modified carbon nanotubes (CNT) as the host to covalently bind sulfur and confirmed that the prepared copolymer can suppress the shuttle effect by covalent interaction between thiol groups and sulfur and soluble polysulfides.[22] However, the limited number of functional groups grafted on the carbon matrix leads to ineffective inhibition of the polysulfide shuttling.

Metal-organic frameworks (MOFs), which are characterized by adjustable functional organic ligands, large specific surface area and regular pore structure, providing opportunities to construct advanced cathode for Li-S batteries. [23-28] For example, Zhang et al. prepared a thiol-modified MOF by post-synthesis grafting thiol groups onto UiO-66-NH_2 and verify the covalent connection between thiol-modified MOF and sulfur by systematic characterization.[29] Nevertheless, each linker in this thiol-modified MOF bears only one thiol group and the potential of functional linker has not been fully tapped. Moreover, the synthesis of the thiol-modified MOF involves a complicated graft process to obtain desired functional groups and the reaction kinetics of Li-S cells with thiol MOF-sulfur copolymer is still unexplored.

In this work, we synthesized a dual-thiol MOF-decorated CNT (UiO-66(SH)$_2$@CNT) via a simple one-step solvothermal process and used it to covalently bind with sulfur to form MOF-sulfur copolymer (S-UiO-66(SH)$_2$@CNT). As illustrated in Figure 1, the S-UiO-66(SH)$_2$@CNT can efficiently restrain the shuttle of polysulfides by covalent connecting thiol-rich UiO-66(SH)$_2$ to sulfur species. In addition, CNTs was introduced to enhance the conductivity of MOF and the resultant S-UiO-66(SH)$_2$@CNT can accelerate the redox kinetics of polysulfides. Compared with the Li-S cell using the blend of UiO-66@CNT and sulfur as the cathode (S/UiO-66@CNT), the S-UiO-66(SH)$_2$@CNT based cell exhibited better electrochemical performance such as higher discharge capacity and better cycling stability.

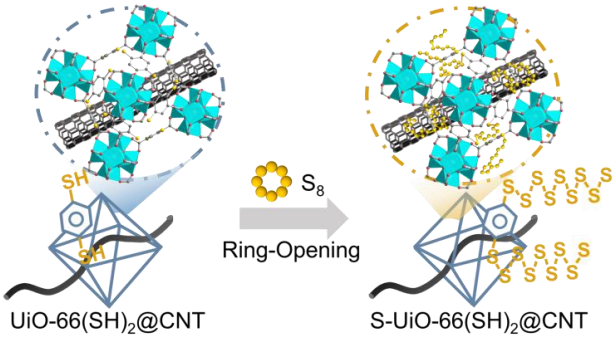

Figure 1. Synthesis route for S-UiO-66(SH)$_2$@CNT.

Experimental

UiO-66(SH)$_2$@CNT was prepared via a one-step hydrothermal approach. Briefly, 2,5-dimercaptoterephthalic acid (H_2DMBD, 38 mg), $ZrCl_4$ (38 mg), acetic acid (1.5 mL), dimethylformamide (DMF, 6.4 mL), and carboxylated CNT (32 mg) were mixed in a Teflon-lined stainless steel autoclave. Then, heat treatment was carried out at 120 °C for 24 hours. Finally, the black UiO-66(SH)$_2$@CNT was obtained after the washing and drying process. For comparison, UiO-66@CNT was fabricated by a similar method applying 1,4-benzenedicarboxylic acid (BDC) in place of H_2DMBD.

The S-UiO-66(SH)$_2$@CNT cathode was prepared by the previously reported method. Sulfur and UiO-66(SH)$_2$@CNT were mixed at a mass ratio of 6:4, and the mixture was heated at 185 °C for 1 day to obtain S-UiO-66(SH)$_2$@CNT. S/UiO-66@CNT was prepared by heating the corresponding composite at 155 °C for 24 hours. Then, the sulfur cathode was fabricated by pasting the slurry comprising 80 wt% active materials, 10 wt% carbon black, and 10 wt% binder onto the aluminum foil. A lithium tablet was used as the anode and the common ether-based electrolyte was used as received. The sulfur loading was controlled to be about 1 mg cm^{-2}.

X-ray diffraction (XRD) pattern was collected with an X-ray powder diffractometer (Rigaku SmartLab). Fourier transform infrared (FT-IR) spectrometry was performed using a spectrometer (Nicolet iS50R). The morphologies of two composites were examined by scanning electron microscopy (SEM, Hitachi 4300N). Thermogravimetric analysis (TGA) was performed with a thermos gravimetric analyzer (STA449F5). The cycling measurement was carried out on a battery tester (Neware BTS-CT-3008-TC). Electrochemical impedance spectroscopy (EIS) test was performed on a workstation (Donghua DH7003).

Results and Discussion

XRD measurements were first applied to evaluate the crystallization of the samples. As displayed in Figure 2, the XRD patterns of UiO-66(SH)$_2$@CNT and UiO-66@CNT display two peaks at 7.4° and 8.5° , which ascribe to the (110) and (200) planes of UiO-66.[30] Also, the patterns of both samples have similar peaks as simulated UiO-66 and show a CNT peak at 26.2° , confirming the incorporation of additional CNT does not disturb the crystal structure of pristine MOFs. TGA was applied to analyze the thermal degradation process of UiO-66@CNT and UiO-66(SH)$_2$@CNT. Specifically, two samples were heated at a heating rate of 10 °C min^{-1} until 800 °C, and nitrogen was used as the purge gas atmosphere. As seen in Figure 3, UiO-66@CNT has an excellent thermal stability up to 450 °C and UiO-66(SH)$_2$@CNT remains stable above 210 °C.

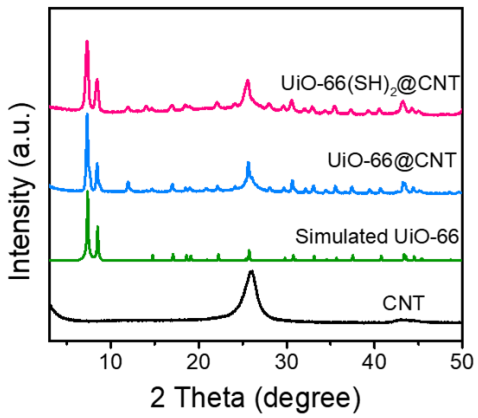

Figure 2. XRD patterns of UiO-66(SH)$_2$@CNT, UiO-66@CNT, simulated UiO-66 and CNT.

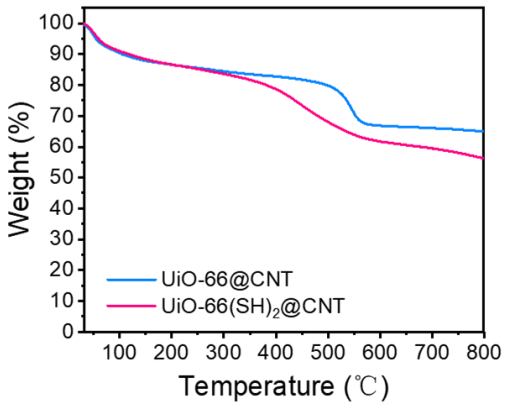

Figure 3. TGA curves of UiO-66@CNT and UiO-66(SH)$_2$@CNT.

FT-IR technique was further used to validate the chemical composition of UiO-66@CNT and UiO-66(SH)$_2$@CNT. As shown in Figure 4, two characteristic peaks at about 1653 and 1585 cm^{-1} confirm the interaction between the Zr node and the carboxyl in two UiO-66-type MOFs.[31] Besides, compared with the spectrum of UiO-66@CNT, a new characteristic peak of the thiol groups (-SH) can be seen in the spectrum of UiO-66(SH)$_2$@CNT.[32] Subsequently, S-UiO-66(SH)$_2$@CNT was prepared by covalent connection between sulfur powder and UiO-66(SH)$_2$@CNT. When the mixture of sulfur and UiO-66(SH)$_2$@CNT was heated at 185 °C, the circular S_8 could cleave into linear sulfur species with radical chain end and covalently connect with UiO-66(SH)$_2$ to form a MOF-sulfur copolymer. In the FT-IR spectrum of S-UiO-66(SH)$_2$@CNT, the absorption peak of -SH almost disappeared. Moreover, the absorption peak at 660 cm^{-1} in UiO-66(SH)$_2$@CNT blue-shifts to 680 cm^{-1} in S-UiO-66(SH)$_2$@CNT, which can be attributed to the formation of C-S bonds according to the previously studies.[33] These results verify that ring-opened linear sulfur species is successfully grafted onto the thiol groups in UiO-66(SH)$_2$@CNT.

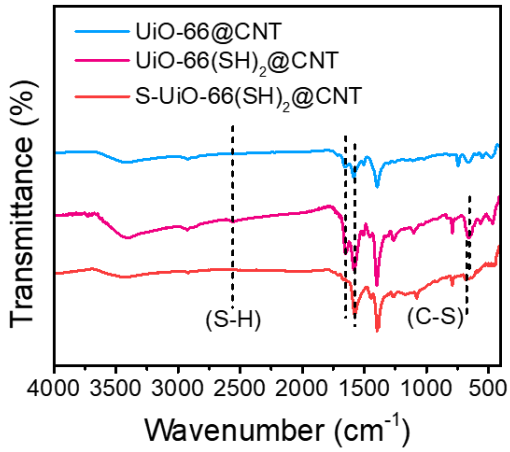

Figure 4. FT-IR spectra of UiO-66@CNT, UiO-66(SH)$_2$@CNT and S-UiO-66(SH)$_2$@CNT.

The morphologies of the prepared UiO-66@CNT and UiO-66(SH)$_2$@CNT were examined by SEM. Because of abundant nucleation sites on the surface of carboxylated CNT, UiO-66 and UiO-66(SH)$_2$ will grow and aggregate out the CNT surface. The loose chained and threaded structure of

UiO-66@CNT and UiO-66(SH)$_2$@CNT is shown in Figure 5. It can be seen that the diameters of UiO-66 and UiO-66(SH)$_2$ nanoparticles are about 46 and 26 nm, and these MOF nanoparticles are strung into a network by CNT. Notably, this network structure not only improves the electrical conductivity of UiO-66 and UiO-66(SH)$_2$ but also avoids the aggregation of MOF nanoparticles, which is expected to be effective for providing more sites for tethering linear sulfur species.

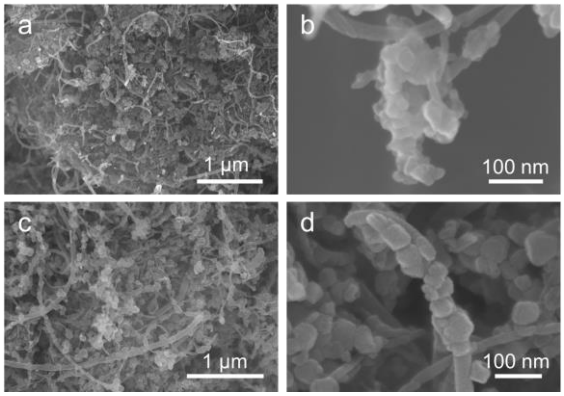

Figure 5. SEM images of (a, b) UiO-66@CNT and (c, d) UiO-66(SH)$_2$@CNT.

To evaluate the advantages of UiO-66(SH)$_2$@CNT, CR2025 coin-type Li-S cells with S-UiO-66(SH)$_2$@CNT cathode were assembled. For comparison, the S/UiO-66@CNT cathode was also prepared by the traditional melt-diffusion method. Firstly, the cyclic stability of Li-S cells with S/UiO-66@CNT and S-UiO-66(SH)$_2$@CNT cathodes were tested within a cutoff voltage window of 1.7–2.8 V. After one cycle activation at 0.2 C, the Li-S cells with two cathodes were cycled at 0.5 C. As shown in Figure 6, the S/UiO-66@CNT cathode exhibits a discharge capacity of 670 mAh g^{-1} at 0.2 C, while the S-UiO-66(SH)$_2$@CNT cathode yields a higher capacity of 791 mAh g^{-1} at the same current density, indicating that the sulfur species are well confined within the S-UiO-66(SH)$_2$@CNT cathode and the utilization of sulfur is greatly increased, which is enabled by rich thiol groups by trapping sulfur and polysulfides. The initial discharge capacity of the Li-S cells with S-UiO-66(SH)$_2$@CNT cathode was 568 mAh g^{-1} at 0.5 C and the capacity was increased to 684 mAh g^{-1} after a slow activation process. The reversible capacity reached 638 mAh g^{-1} with a coulombic efficiency of 96.22 % at the end of 200 cycles, corresponding to a high capacity retention of 93.27 % based on the highest discharge capacity. In comparison, the initial discharge capacity of the Li-S cells with S/UiO-66@CNT cathode was 539 mAh g^{-1} at 0.5 C and the capacity was gradually decreased to 350 mAh g^{-1} with a coulombic efficiency of 95.53 % at the end of 200 cycles, corresponding to a capacity retention of 64.94 %. These results demonstrate that the S-UiO-66(SH)$_2$@CNT cathode possesses a superior cycling performance including higher capacity retention and coulombic efficiency, benefiting from the stable covalent interaction between sulfur species and thiol groups in UiO-66(SH)$_2$.

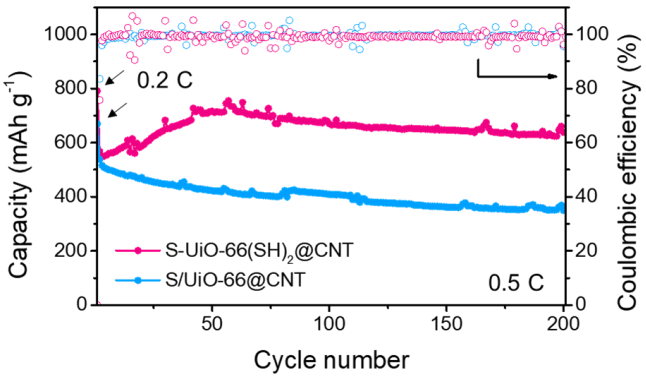

Figure 6. Cyclic stability of Li-S cells with S/UiO-66@CNT and S-UiO-66(SH)$_2$@CNT cathodes at 0.5 C.

Moreover, the galvanostatic charge-discharge performances of Li-S cells with S/UiO-66@CNT and S-UiO-66(SH)$_2$@CNT cathodes at the end of 200 cycles were investigated. As presented in Figure 7, both cathodes show two representative discharge plateaus. The short plateau at the high potential (~2.30 V) corresponds to the reduction of sulfur (S_8) to long-chain polysulfides (Li_2S_n, $3 < n \leq 8$) and the long plateau at the low potential (~2.05 V) suggests the further reduction of soluble polysulfides to solid Li_2S_2 or Li_2S.[34-35] The charge plateau represents the reverse oxidation of Li_2S_2 or Li_2S to S_8. In addition, the high-voltage (C_H) and low-voltage (C_L) plateau capacities are extracted from the discharge curves. The S-UiO-66(SH)$_2$@CNT cathode displays high C_H (264 mAh g^{-1}) and C_L (374 mAh g^{-1}). The lower C_H of 140 mAh g^{-1} and C_L of 210 mAh g^{-1} are obtained for the S/UiO-66@CNT cathode. In addition, the S-UiO-66(SH)$_2$@CNT cathode exhibits a voltage hysteresis of 268.5 mV, which is much smaller than that of the S/UiO-66@CNT cathode (285.8 mV), indicating the accelerated redox kinetics and the strong interaction between thiol groups and sulfur species. In addition, EIS measurement was applied to study the difference in charge transfer. As displayed in Figure 8, the Nyquist plots of two cathodes consist of a semicircle and an inclined line, which represent the charge transfer resistance (R_{ct}) and diffusion impedance of lithium ions, respectively.[36] The S-UiO-66(SH)$_2$@CNT cathode yields a lower R_{ct} (59 Ω) than S/UiO-66@CNT (167 Ω), demonstrating the enhanced charge transferability and accelerated redox kinetics in Li-S with S-UiO-66(SH)$_2$@CNT.

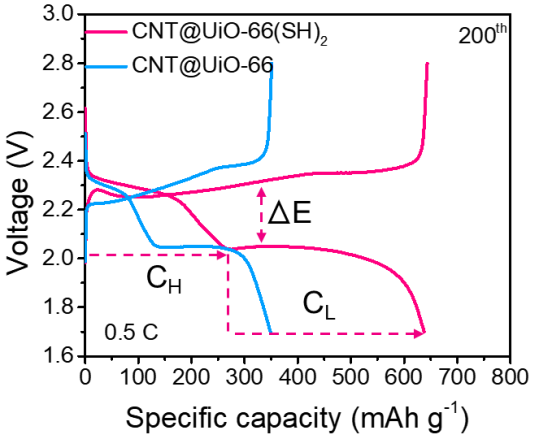

Figure 7. Charge-discharge profiles of S/UiO-66@CNT and S-UiO-66(SH)$_2$@CNT cathodes after 200 cycles at 0.5 C.

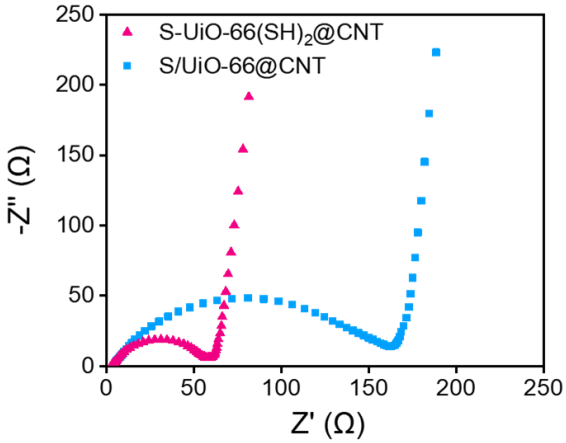

Figure 8. EIS curves of S/UiO-66@CNT and S-UiO-66(SH)$_2$@CNT cathodes.

Conclusions

In summary, a thiol-rich MOF-modified CNT(UiO-66(SH)$_2$@CNT) is synthesized by in situ growth method and used to covalently bind with sulfur to form MOF-sulfur copolymer (S-UiO-66(SH)$_2$@CNT). Benefiting from the covalent connection between sulfur and UiO-66(SH)$_2$@CNT, S-UiO-66(SH)$_2$@CNT could inhibit the shuttle effect and simultaneously promote the conversion kinetics of polysulfides. Consequently, the resultant S-UiO-66(SH)$_2$@CNT cathode exhibits a higher discharge capacity of 791 mAh g^{-1} at 0.2 C and a higher capacity retention of 93.27 % at 0.5 C during 200 cycles compared with that of the S/UiO-66@CNT cathode. The present work may inspire the design of advanced MOFs and cathodes for high performance Li-S batteries.

Acknowledgements

We acknowledge financial support of the National Natural Science Foundation of China (21871061), the Foundation of Basic and Applied Basic Research of Guangdong Province (2020B1515120024), and Local Innovative and Research Teams Project of Guangdong Pearl River Talents Program (2017BT01Z032).

References

[1] Seh, Z. W.; Sun, Y.; Zhang, Q.; Cui, Y. Designing high-energy lithium–sulfur batteries. Chem. Soc. Rev. 2016, 45, 5605-5634.

[2] Pan, Z.; Brett, D. J. L.; He, G.; Parkin, I. P. Progress and Perspectives of Organosulfur for Lithium–Sulfur Batteries. Adv. Energy Mater. 2022, 12, 2103483.

[3] Zhou, G.; Chen, H.; Cui, Y. Formulating energy density for designing practical lithium–sulfur batteries. Nat. Energy 2022, 7, 312-319.

[4] Huang, Y.; Lin, L.; Zhang, C.; Liu, L.; Li, Y.; Qiao, Z.; Lin, J.; Wei, Q.; Wang, L.; Xie, Q.; et al. Recent Advances and Strategies toward Polysulfides Shuttle Inhibition for High-Performance Li–S Batteries. Adv. Sci. 2022, 9, 2106004.

[5] Hu, X.; Huang, T.; Zhang, G.; Lin, S.; Chen, R.; Chung, L.-H.; He, J. Metal-organic framework-based catalysts for lithium-sulfur batteries. Coord. Chem. Rev. 2023, 475, 214879.

[6] Liu, Y.; Meng, X.; Wang, Z.; Qiu, J. Development of quasi-solid-state anode-free high-energy lithium sulfide-based batteries. Nat. Commun. 2022, 13, 4415.

[7] Qiu, W.; Li, G.; Luo, D.; Zhang, Y.; Zhao, Y.; Zhou, G.; Shui, L.; Wang, X.; Chen, Z. Hierarchical Micro-Nanoclusters of Bimetallic Layered Hydroxide Polyhedrons as Advanced Sulfur Reservoir for High-Performance Lithium–Sulfur Batteries. Adv. Sci. 2021, 8, 2003400.

[8] Ye, Z.; Jiang, Y.; Li, L.; Wu, F.; Chen, R. Self-Assembly of 0D–2D Heterostructure Electrocatalyst from MOF and MXene for Boosted Lithium Polysulfide Conversion Reaction. Adv. Mater. 2021, 33, 2101204.

[9] Ye, Z.; Jiang, Y.; Li, L.; Wu, F.; Chen, R. Rational Design of MOF-Based Materials for Next-Generation Rechargeable Batteries. Nano-Micro Lett. 2021, 13, 203.

[10] Chu, Z.; Gao, X.; Wang, C.; Wang, T.; Wang, G. Metal–organic frameworks as separators and electrolytes for lithium–sulfur batteries. J. Mater. Chem. A 2021, 9, 7301-7316.

[11] Qi, F.; Sun, Z.; Fan, X.; Wang, Z.; Shi, Y.; Hu, G.; Li, F. Tunable Interaction between Metal-Organic Frameworks and Electroactive Components in Lithium-Sulfur Batteries: Status and Perspectives. Adv. Energy Mater. 2021, 2100387.

[12] Tian, Y.; Li, G.; Zhang, Y.; Luo, D.; Wang, X.; Zhao, Y.; Liu, H.; Ji, P.; Du, X.; Li, J.; et al. Low-Bandgap Se-Deficient Antimony Selenide as a Multifunctional Polysulfide Barrier toward High-Performance Lithium–Sulfur Batteries. Adv. Mater. 2020, 32, 1904876.

[13] Li, G.; Lu, F.; Dou, X.; Wang, X.; Luo, D.; Sun, H.; Yu, A.; Chen, Z. Polysulfide Regulation by the Zwitterionic Barrier toward Durable Lithium–Sulfur Batteries. J. Am. Chem. Soc. 2020, 142, 3583-3592.

[14] Wang, P.; Xi, B.; Huang, M.; Chen, W.; Feng, J.; Xiong, S. Emerging catalysts to promote kinetics of lithium–sulfur batteries. Adv. Energy Mater. 2021, 11, 2002893.

[15] Zhang, Y.; Zhang, X.; Silva, S. R. P.; Ding, B.; Zhang, P.; Shao, G. Lithium–sulfur batteries meet electrospinning: recent advances and the key parameters for high gravimetric and volume energy density. Adv. Sci. 2022, 9, 2103879.

[16] Xu, J.; An, S.; Song, X.; Cao, Y.; Wang, N.; Qiu, X.; Zhang, Y.; Chen, J.; Duan, X.; Huang, J. Towards High Performance Li-S Batteries via Sulfonate-Rich COF-Modified Separator. Adv. Mater. 2021, 33, 2105178.

[17] Liang, J.; Sun, Z.-H.; Li, F.; Cheng, H.-M. J. E. S. M. Carbon materials for Li–S batteries: Functional evolution and performance improvement. Energy Storage Mater. 2016, 2, 76-106.

[18] Zhang, L.; Wang, Y.; Niu, Z.; Chen, J. Advanced nanostructured carbon-based materials for rechargeable lithium-sulfur batteries. Carbon 2019, 141, 400-416.

[19] Li, M.; Zhou, X.; Ma, X.; Chen, L.; Zhang, D.; Xu, S.; Duan, D.; Chen, C.; Yuan, Q.; Liu, S. Development of sulfonated-carbon nanotubes/graphene three-dimensional conductive spongy framework with ion-selective effect as cathode in high-performance lithium-sulfur batteries. Chem. Eng. J. 2021, 409, 128164.

[20] Deng, N.; Liu, Y.; Li, Q.; Yan, J.; Lei, W.; Wang, G.; Wang, L.; Liang, Y.; Kang, W.; Cheng, B. Functional mechanism analysis and customized structure design of interlayers for high performance Li-S battery. Energy Storage Mater. 2019, 23, 314-349.

[21] Xu, N.; Qian, T.; Liu, X.; Liu, J.; Chen, Y.; Yan, C. Greatly suppressed shuttle effect for improved lithium sulfur battery performance through short chain intermediates. Nano Lett. 2017, 17, 538-543.

[22] Xu, Y.-W.; Zhang, B.-H.; Li, G.-R.; Liu, S.; Gao, X.-P. Covalently bonded sulfur anchored with thiol-modified carbon nanotube as a cathode material for lithium–sulfur batteries. ACS Appl. Energy Mater. 2019, 3, 487-494.

[23] Zheng, Y.; Zheng, S.; Xue, H.; Pang, H. Metal–organic frameworks for lithium–sulfur batteries. J. Mater. Chem. A 2019, 7, 3469-3491.

[24] Li, C.; Liu, R.; Xiao, Y.; Cao, F.; Zhang, H. Recent progress of separators in lithium-sulfur batteries. Energy Storage Mater. 2021,

40, 439-460.
[25] Zhou, C.; Li, Z.; Xu, X.; Mai, L. Metal-organic frameworks enable broad strategies for lithium-sulfur batteries. Natl. Sci. Rev. 2021, 8, nwab055.
[26] Ye, Z.; Jiang, Y.; Li, L.; Wu, F.; Chen, R. Rational Design of MOF-Based Materials for Next-Generation Rechargeable Batteries. Nano-Micro Letters 2021, 13.
[27] Zheng, Z.-J.; Ye, H.; Guo, Z.-P. Recent progress on pristine metal/covalent-organic frameworks and their composites for lithium–sulfur batteries. Energy Environ. Sci. 2021, 14, 1835-1853.
[28] Zhao, R.; Liang, Z.; Zou, R.; Xu, Q. Metal-organic frameworks for batteries. Joule 2018, 2, 2235-2259.
[29] Liu, X.; Wang, S.; Wang, A.; Wang, Z.; Chen, J.; Zeng, Q.; Chen, P.; Liu, W.; Li, Z.; Zhang, L. A new cathode material synthesized by a thiol-modified metal–organic framework (MOF) covalently connecting sulfur for superior long-cycling stability in lithium–sulfur batteries. J. Mater. Chem. A 2019, 7, 24515-24523.
[30] Wang, X.; Yang, G.; Chai, G.; Nasir, M. S.; Wang, S.; Zheng, X.; Wang, C.; Yan, W. Fabrication of heterostructured UIO-66-NH_2/CNTs with enhanced activity and selectivity over photocatalytic CO2 reduction. Int. J. Hydrogen Energy 2020, 45, 30634-30646.
[31] Fu, L.; Wang, S.; Lin, G.; Zhang, L.; Liu, Q.; Fang, J.; Wei, C.; Liu, G. Post-functionalization of UiO-66-NH_2 by 2, 5-Dimercapto-1, 3, 4-thiadiazole for the high efficient removal of Hg (II) in water. J. Hazard. Mater. 2019, 368, 42-51.
[32] Hu, X.; Lin, S.; Chen, R.; Zhang, G.; Huang, T.; Li, J.; Yang, X.; Chung, L.-H.; Yu, L.; He, J. Thiol-Containing Metal–Organic Framework-Decorated Carbon Cloth as an Integrated Interlayer–Current Collector for Enhanced Li–S Batteries. ACS Appl. Mater. Interfaces 2022, 14, 31942-31950.
[33] Zeng, Q.; Li, X.; Gong, W.; Guo, S.; Ouyang, Y.; Li, D.; Xiao, Y.; Tan, C.; Xie, L.; Lu, H. Copolymerization of Sulfur Chains with Vinyl Functionalized Metal−Organic Framework for Accelerating Redox Kinetics in Lithium−Sulfur Batteries. Adv. Energy Mater. 2022, 12, 2104074.
[34] Chu, F.; Wang, M.; Liu, J.; Guan, Z.; Yu, H.; Liu, B.; Wu, F. Low Concentration Electrolyte Enabling Cryogenic Lithium–Sulfur Batteries. Adv. Funct. Mater. 2022, 32, 2205393.
[35] Xiao, C.; Song, W.; Liang, J.; Zhang, J.; Huang, Z.; Zhang, J.; Wang, H.; Zhong, C.; Ding, J.; Hu, W. P-block tin single atom catalyst for improved electrochemistry in a lithium–sulfur battery: a theoretical and experimental study. J. Mater. Chem. A 2022, 10, 3667-3677.
[36] Chu, R.; Nguyen, T. T.; Bai, Y.; Kim, N. H.; Lee, J. H. Uniformly Controlled Treble Boundary Using Enriched Adsorption Sites and Accelerated Catalyst Cathode for Robust Lithium–Sulfur Batteries. Adv. Energy Mater. 2022, 2102805.